

Probing a Mixed Neutralino Dark Matter Model at the 7 TeV LHC

Monoranjan Guchait^a, D.P. Roy^b, Dipan Sengupta^a

^a *Department of High Energy Physics
Tata Institute of Fundamental Research
Homi Bhabha Road, Mumbai-400005, India.*

^b *Homi Bhabha's Centre for Science Education
Tata Institute of Fundamental Research
V. N. Purav Marg, Mumbai-400088, India.*

Abstract

We have analyzed the prospect of probing a non-universal gaugino mass model of mixed bino-higgsino dark matter at the current 7 TeV run of LHC. It provides cosmologically compatible dark matter relic density over two broad bands of parameters, corresponding to $m_{\tilde{g}} < m_{\tilde{q}}$ and $m_{\tilde{g}} \sim m_{\tilde{q}}$. The SUSY spectrum of this model has two distinctive features : (i) an approximate degeneracy among the lighter chargino and neutralino masses, and (ii) an inverted mass hierarchy of squark masses. We find that these features can be exploited to obtain a viable signal upto $m_{\tilde{g}} \sim 800$ GeV over both the parameter bands with an integrated luminosity $5fb^{-1}$.

1 Introduction

Supersymmetry is a very popular and well motivated extension of the Standard Model(SM) as it provides a natural solution to the gauge hierarchy problem of the SM along with a natural candidate for the dark matter(DM) of the universe. This has led to an intense global search for supersymmetry(SUSY) in the colliders as well as the dark matter experiments, which are both going through rapid developments. The CERN Large Hadron Collider(LHC) has already accumulated a luminosity of 3 fb^{-1} at a CM energy of 7 TeV, which is expected to go up to 5 fb^{-1} by the end of this year and $10\text{-}15\text{ fb}^{-1}$ by the end of the current run in late 2012. After this the machine is scheduled to be upgraded to run at the designed CM energy of 14 TeV starting in 2015. Then one can probe most of the interesting parameter space of supersymmetry and in particular the minimal supersymmetric standard model(MSSM). Likewise direct DM detection experiments like XENON100 and Super CDMS as well as the indirect detection experiment like Ice Cube and Fermi-LAT are expected to probe significant parts of the MSSM parameter space over the next 4-5 years. It is well known now that the so called constrained MSSM or the minimal supergravity(mSUGRA) model corresponds to a dominantly bino DM, resulting in a generic overabundance of relic density. There are only a few narrow strips of the mSUGRA parameter space that correspond to cosmologically compatible DM relic density. It will be possible to probe these cosmologically compatible regions of mSUGRA parameter space at the 14 TeV runs of LHC, but not at the 7 TeV. In fact the 7 TeV run of LHC is expected to probe only a limited region of the mSUGRA parameter space, much of which is already excluded by the Higgs mass limit from LEP [1, 2].

Moreover, much of these cosmologically compatible parameter regions of mSUGRA model will be hard to probe at the above mentioned DM experiments. On the other hand there are simple and well motivated versions of MSSM with non-universal gaugino masses at the GUT scale, which correspond to mixed bino-higgsino dark matter. They lead to cosmologically compatible DM relic density over large parts of parameter space and also promising signals in the above mentioned DM experiments. In this paper we shall study the prospect of probing such a mixed bino-higgsino dark matter model at the current 7 TeV run of LHC. We find a promising signal for this model over a significant part of the cosmologically compatible parameter space.

In section 2 we summarize the essential features of the two non-universal gaugino mass models with mixed neutralino dark matter, which give cosmologically compatible relic density along with promising direct detection signals over large parts of their parameter space. We briefly discuss these features and for one of them, which corresponds to a relatively light gluino and hence a promising signal at 7 TeV. In section 3 we study in detail the signal cross sections along with the relevant SM backgrounds in jets + missing transverse energy(\cancel{E}_T) as well as leptonic channels. We conclude with a brief summary of our results in section 4.

2 Non-universal Gaugino mass Models for Mixed Neutralino DM

These models are based on the assumption that SUSY is broken by an admixture of two superfields belonging to a singlet and a non-singlet representation of the GUT group which is SU(5) for the simplest case [3]. The gauge kinetic function responsible for the GUT scale gaugino masses originates from the vacuum expectation value of the F term of a chiral superfield Φ responsible for SUSY breaking,

$$\frac{\langle F_\Phi \rangle}{M_{Plank}} \lambda_i \lambda_j \quad (1)$$

where $\lambda_{1,2,3}$ are the U(1), SU(2), SU(3) gaugino fields - bino, wino and gluino. Since the gauginos belong to the adjoint representation of the GUT group SU(5), Φ and F_Φ can belong to any of the irreducible representations appearing in their symmetric product.

$$(24 \times 24)_{sym} = 1 + 24 + 75 + 200. \quad (2)$$

Thus the GUT scale gaugino masses for a given representation are determined in terms of a given SUSY breaking mass parameter by

$$M_{1,2,3}^G = C_{1,2,3}^n m_{1/2}^n \quad (3)$$

where,

$$C_{1,2,3}^1 = (1, 1, 1); C_{1,2,3}^{24} = (-1, -3, 2); C_{1,2,3}^{75} = (-5, 3, 1); C_{1,2,3}^{200} = (10, 2, 1). \quad (4)$$

The mSUGRA model assumes Φ to be a singlet, leading to universal gaugino masses at the GUT scale. On the other hand any of the non-singlet representations for Φ would imply non-universal gaugino masses as per eqs. 3 and 4. The phenomenology of such non-universal gaugino mass models have been extensively studied in the literature [4, 5, 6, 7, 8]. Since the gaugino masses evolve like the corresponding gauge couplings at the one-loop level of the RGE, the three gaugino masses are proportional to the respective gauge couplings, i.e,

$$\begin{aligned} M_1 &= (\alpha_1/\alpha_G) M_1^G \simeq (25/60) C_1^n m_{1/2}^n, \\ M_2 &= (\alpha_2/\alpha_G) M_2^G \simeq (25/30) C_2^n m_{1/2}^n, \\ M_3 &= (\alpha_3/\alpha_G) M_3^G \simeq (25/9) C_3^n m_{1/2}^n. \end{aligned} \quad (5)$$

The higgsino mass parameter μ is obtained from the electro-weak(EW) symmetry breaking condition along with the one loop RGE for the Higgs scalar mass, i.e,

$$\mu^2 + M_Z^2/2 \simeq -m_{H_u}^2 \simeq -0.1m_0^2 + 2.1M_3^{G^2} - 0.22M_2^{G^2} + 0.19M_2^G M_3^G \quad (6)$$

neglecting the contribution from the GUT scale trilinear coupling term A_0 [9]. The numerical co-efficients on the right correspond to a representative value of $\tan \beta = 10$; but they show

only mild variation over the moderate $\tan\beta$ region.

Although we use exact numerical solutions to the two-loop RGE in our analysis, the composition of the lightest neutralino DM χ_1^0 can be seen from the relative values of the gaugino and higgsino masses, given by eqs. 3-5 and eq.6 respectively. For the mSUGRA(singlet Φ), one gets $M_1 < \mu$, resulting in a bino DM over most of the parameter space. Since bino has no gauge charge it can only pair annihilate via sfermion exchange and the large sfermion mass limit from LEP [10] leads to overabundance of DM relic density. The same is true for the 24-plet representation. On the other hand, the 75 and 200 plet representations imply $M_{1,2} > \mu$, leading to higgsino DM over most of the parameter space, and since the higgsino DM can effectively co-annihilate with its nearly degenerate chargino via W-boson exchange, one gets a generic underabundance of DM relic density for these two representations [5]. Finally, assuming the SUSY breaking to occur via an admixture of a singlet and a non-singlet superfield belonging to the (1+75) or (1+200) representations [6, 7], i.e,

$$\begin{aligned} m_{1/2}^1 &= (1 - \alpha_{75})m_{1/2}; & m_{1/2}^{75} &= \alpha_{75}m_{1/2}, \\ m_{1/2}^1 &= (1 - \alpha_{200})m_{1/2}; & m_{1/2}^{200} &= \alpha_{200}m_{1/2}, \end{aligned} \quad (7)$$

one can get large admixture of gaugino and higgsino components in the DM. It was shown in [7] that one gets optimal admixture of bino and higgsino components in the (1+75) model and bino, wino, higgsino components in the (1+200) model with $\alpha_{75} = 0.475$ and $\alpha_{200} = 0.12$, leading to WMAP [11] satisfying DM relic density over large parts of the MSSM parameter space. They are two simple realizations of the so called well tempered neutralino scenario[12]. Once the mixing parameter is fixed, each of these models is as predictive as mSUGRA model. The WMAP satisfying DM relic density region of the (1+200) model correspond to relatively heavy gluino and squark masses in the TeV range, which is inaccessible at the 7 TeV run. We therefore concentrate on the (1+75) model.

The large admixture of the bino and the higgsino components of the DM in this model leads to promising signals for the direct detection experiments as well as indirect detection experiments like Ice Cube [7]. In particular, the model prediction was shown to agree with the putative direct DM signal, corresponding to the two CDMS II candidate events [13], over the relatively low DM mass region [8]. Figure 1 compares the model prediction with the putative signal corridor, represented by the central value and the 90% upper and lower limits corresponding to the two CDMS II candidate events. The 90% upper limit of the more recent XENON100 experiments [14] is overlayed on this figure for comparison. One sees that the central value curve of the two CDMS II candidate events is in conflict with the XENON100 upper limit, which lies marginally below it. However there are only very few points of the model parameter scan that overlap with this central value. Most of the points are crowded near the lower limit of the putative signal corridor of the two CDMS II candidate events, which are also compatible with the XENON100 upper limit. One expects this part of the model prediction to be tested by the XENON100 and the super CDMS

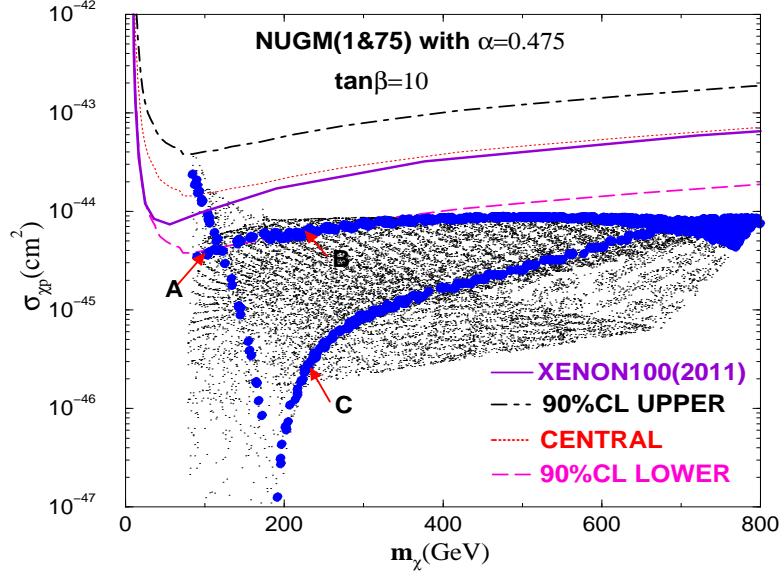


Figure 1: Prediction of the (1+75) model compared with the putative signal corridor corresponding to the two candidate DM scattering events of the CDMS II experimental [13]. The 90% C.L. upper limit of the recent XENON100 experiments [14] is overlayed as the solid line. The blue(dark) dots corresponding the WMAP relic density satisfying region of the model. The three representative points A,B and C are shown in the low mass part of the region which is accessible to the 7 TeV LHC run.

experiments over the next few years. It is therefore very pertinent to find out if this part of the model parameter space can be probed at the current LHC run. It should be noted here that the upper band of the WMAP relic density compatible points of the (1+75) model shown in figure 1 corresponds to a DM with comparable bino and higgsino components, which annihilate via(s and t channel) gauge boson exchange processes

$$\chi_1^0 \chi_1^0, \chi_1^0 \chi_2^0, \chi_1^0 \chi_1^\pm \rightarrow WW, ZZ, f\bar{f}. \quad (8)$$

On the other hand, the lower band of the WMAP relic density compatible points corresponds to a DM with $\leq 10\%$ higgsino component, which annihilate via s channel Higgs exchange processes[8]

$$\chi_1^0 \chi_1^0, \chi_1^0 \chi_2^0, \chi_1^0 \chi_1^\pm \rightarrow t\bar{t}, b\bar{b}, \tau\bar{\tau}, t\bar{b}, \tau\nu_\tau. \quad (9)$$

The comparable gaugino and higgsino components of the DM for the upper branch accounts for the large spin independent χp scattering cross section, while the low higgsino component of DM in the lower branch accounts for the low χp cross section. Therefore, it will be more difficult to probe the parameter space corresponding to lower branch in direct DM detection experiments. On the other hand both the branches can be probed at the 7 TeV LHC run up to a gluino mass of ~ 800 GeV corresponding to $m_\chi \sim 250$ GeV. In fact the

Model	\tilde{g}	\tilde{q}_L	\tilde{q}_R	\tilde{t}_1	\tilde{b}_1	\tilde{e}_l	$\tilde{\tau}_1$	χ_1^0	χ_2^0	χ_1^+	χ_2^+
A	433	1280	1274	759	1054	1263	1246	104	122	123	271
B	793	1480	1440	902	1246	1375	1327	227	256	257	501
C	722	750	660	483	649	437	237	231	301	302	490

Table 1: Mass spectrum(in GeV) for the three representative parameter points (A) $m_{1/2}=144$ GeV, $m_0=1255$ GeV, (B) $m_{1/2}=300$ GeV, $m_0=1325$ GeV, (C) $m_{1/2}=300$ GeV, $m_0=185$ GeV.

lower branch will be easier to probe since the corresponding cross section is larger due to the lower squark masses($m_{\tilde{q}} \sim m_{\tilde{g}}$) as we shall see below. Therefore we have selected two representative points on the upper branch along with one on the lower branch spanning the above mentioned gluino mass range. In the next section we shall investigate in detail the 7 TeV LHC signals corresponding to these three representative points in the parameter space of interest along with relevant backgrounds.

3 The expected model signals and backgrounds in the 7 TeV LHC run

In table 1, we show the mass spectrum of SUSY particles at the electro-weak scale for the three representative points A, B and C marked in figure 1. Table 2 shows the corresponding decay branching ratios. We use the **SuSpect-SUSYHIT** [15] to generate the SUSY spectra and branching ratios. We see from table 1 that the SUSY spectrum of the (1+75) model has two distinctive features vis a vis the mSUGRA model -(1) a near degeneracy of the lighter neutralino and chargino($\chi_1^0, \chi_2^0, \chi_1^\pm$) masses and (2) inverted hierarchy of the squark masses where in particular \tilde{t}_1 is significantly lighter than the other squarks. Indeed both the features are common to most mixed neutralino DM models. The 1st feature implies that χ_1^0 coming from the SUSY cascade decay carries a relatively a large fraction of the energy-momentum, resulting in a hard missing transverse energy (E_T) distribution. The 2nd feature implies that the gluino decays preferentially to t and b quarks leading to several hard isolated leptons and b-tags along with the large E_T . These features make the LHC signal for the mixed neutralino DM model more promising in comparison to the much studied mSUGRA model. Table 2 shows that point A has a large two body decay $\tilde{g} \rightarrow g\chi_{2,3}^0$. This arises via the the virtual $t\bar{t}$ channel since the $t\bar{t}\chi_1^0$ channel is kinetically forbidden in this case. However the decay channels

$$\tilde{g} \rightarrow t\bar{t}\chi_i^0, \bar{t}b(t\bar{b})\chi_1^\pm, b\bar{b}\chi_2^0 \quad (10)$$

account for 83% for point B and 57% for point C. Therefore one can effectively enhance the $\tilde{g}\tilde{g}$ pair production signal over background by demanding ≥ 3 b-tags. As we shall see below,

Decays	A	B	C
$\tilde{g} \rightarrow \tilde{q}q$			43%
$\tilde{g} \rightarrow \tilde{b}b$			17%
$\tilde{g} \rightarrow \tilde{t}t$			40%
$\tilde{t}_1 \rightarrow b\chi_1^\pm$			88%
$\tilde{q}_L \rightarrow q\chi_{1,2}^\pm$			62%
$\tilde{q}_L \rightarrow q\chi_{1,2,3,4}^0$			32%
$\tilde{g} \rightarrow t\bar{b}\chi_1^\pm$	25%	54%	
$\tilde{g} \rightarrow g\chi_{2,3}^0$	30%	4.2%	
$\tilde{g} \rightarrow q\bar{q}\chi_{1,2}^\pm$	16%	2.6%	
$\tilde{g} \rightarrow b\bar{b}\chi_{1,2,3,4}^0$	12%	2%	
$\tilde{g} \rightarrow t\bar{t}\chi_{1,2,3,4}^0$		27%	
$\tilde{g} \rightarrow q\bar{q}\chi_{1,2,3,4}^0$	17%	2%	
$\chi_1^+ \rightarrow q\bar{q}\chi_1^0$	68%	67%	
$\chi_1^+ \rightarrow e\bar{e}\chi_1^0$	22%	22%	
$\chi_1^+ \rightarrow \tilde{\tau}\nu_\tau$			100%
$\chi_2^0 \rightarrow q\bar{q}\chi_1^0$	68%	66%	
$\chi_2^0 \rightarrow \tilde{\tau}_1\tau$			84%
$\chi_2^0 \rightarrow \tilde{e}e$			16%

Table 2: Decay branching ratios of sparticles for three representative points A, B and C, as shown in table 1.

this is particularly useful for the point B where the SUSY signal is dominated by $\tilde{g}\tilde{g}$ pair production. The pair production cross sections of strong SUSY particles, $\tilde{g}\tilde{g}, \tilde{q}\tilde{q}, \tilde{q}\tilde{q}, \tilde{q}\tilde{q}^*$ are calculated using **Prospino** [16] at the NLO level.

The signal and background events are simulated using **PYTHIA** [17] interfacing with fast detector simulation package **PGS** [18]. In **PGS** jets are reconstructed using cone algorithm with cone size $\Delta R = 0.5$, taking inputs from the energy deposits in the calorimeter cells. In the simulation jets are selected with

$$p_T^j \geq 30 \text{ GeV}; |\eta^j| \leq 3.0. \quad (11)$$

We select leptons (e and μ) with

$$p_T^\ell \geq 10 \text{ GeV}; |\eta^\ell| \leq 2.5, \quad (12)$$

and for di-lepton final state leading lepton to pass a cut

$$p_T^{\ell_1} \geq 20 \text{ GeV}. \quad (13)$$

The isolation of lepton is ensured by looking at the total transverse energy $E_T^{ac} \leq 20\%$ of the p_T of lepton, where E_T^{ac} is the scalar sum of transverse energies of jets within a cone of size $\Delta R(l, j) \leq 0.2$ between jet and lepton. In **PGS** the missing transverse energy (\cancel{E}_T) is measured using the toy calorimeter informations. While the use of exact b-tagging method is out of the scope of this work, the b jet candidate is identified by performing a matching between a b quark and jet with a matching cone $\Delta R = 0.3$. The selected 3 and 4 b jets events are multiplied by efficiency factors $\epsilon_b^3 = 0.21$ and $4\epsilon_b^3 - 3\epsilon_b^4 = 0.47$ for ≥ 3 b-tags assuming b tagging efficiency $\epsilon_b = 0.6$ [19]. The dominant SM backgrounds corresponding to signal originate from the $t\bar{t}$ and QCD processes. We have checked also other SM processes like, $W/Z + \text{jets}$, WW, WZ, ZZ , whose contribution to the total background cross section is found to be negligible after applying selection cuts. We investigate the discovery potential of the signal for this mixed neutralino DM model in the di-lepton and single lepton channels including jets plus \cancel{E}_T . We also analyze the inclusive jets + \cancel{E}_T signal which is expected to give better sensitivity. As explained above, we require ≥ 3 b-tagged jets for single lepton and jets + \cancel{E}_T final states to suppress SM backgrounds mainly from $t\bar{t}$. In the following we describe search strategies for all the three channels.

Di-lepton + jets + \cancel{E}_T : In the di-lepton channel we select both same sign(SS) and opposite sign(OS) leptons passed by lepton cuts, eqs. 12, 13. In addition, these events are also subject to following kinematic cuts to suppress SM backgrounds,

$$\begin{aligned} \text{Number of jets} &\geq 3; \cancel{E}_T \geq 100 \text{ GeV}, \\ M_{eff} &\geq 500 \text{ GeV}; R_{\ell\ell} \leq 0.25, \\ m_{\ell\ell} &\neq 75 - 110 \text{ GeV for OS leptons}, \end{aligned} \quad (14)$$

Proc	C.S (pb)	N_{ev}	2ℓ & $n_j \geq 3$	$E_T \geq$ 100	M_{eff} ≥ 500	$R_{ll} \leq$ 0.25	SS,OS	$m_{\ell\ell}$ $\neq 75-110$	$1fb^{-1}$ SS OS	$5fb^{-1}$ SS OS
A: $\tilde{g}\tilde{g}$	5.84	10k	185	134	75	61	16,45	16,36	10.0,21.0	50.,105
A: $\tilde{q}\tilde{q}$	0.28	10k	342	303	301	279	89,190	89,150	2.5, 4.2	12.5,23
Total									12.5,25.2	62.5,126.0
B: $\tilde{g}\tilde{g}$	0.06	10k	737	609	503	382	142,240	142,198	1.0,1.3	5,6.5
B: $\tilde{q}\tilde{q}$	0.018	10k	492	359	317	290	12,188	12,111	0.,2	0.,1.0
Total									1.0, 1.5	5.,7.5
C: $\tilde{g}\tilde{g}$	0.1	10k	401	351	306	233	41,192	41,135	0.6,1.5	3.0,7.5
C: $\tilde{q}\tilde{q}$	0.57	10k	492	359	317	290	12,188	12,111	0.75,6.3	3.75,31.5
C: $\tilde{q}\tilde{q}$	0.55	10k	395	348	333	234	13,221	13,145	0.8,8	4.,40.
Total									2.15,15.8	10.75,79
$t\bar{t}$										
5 – 200	143.5	100k	227	78	31	13	2,11	2,9	6.0,21.0	30.,105
200-500	16.3	50k	292	145	87	33	5,28	5,22	2.5, 10.7	12.5,53.5
500-inf	0.16	10k	87	65	63	26	6,20	6,19	0.5,1.3	2.5, 6.5
Total									9.0,33.0	45.0,165.0
QCD										
200-300	6983	1M	1	1	0	0	0,0	0,0	0,0	0.,0.
300-500	873	1M	15	2	2	1	1,0	1,0	0.9,0	4.5.,0.
500-800	43.1	100k	4	2	2	0	0,0	0,0	0,0	0.,0.
Total									0.9,0.0	4.5,0.

Table 3: The signal and SM background events for di-lepton final states. The $t\bar{t}$ and QCD backgrounds events are simulated for different \hat{p}_T bins as shown. In the case of $t\bar{t}$ background, we multiply cross sections by the K-factor 1.6 to take into account NLO effects [20]. (Energy units are in GeV).

where effective mass of the event $M_{eff} = \sum_{j=1}^3 p_T^j + E_T$ and $R_{\ell\ell} = \frac{P_T^{\ell_1} + P_T^{\ell_2}}{H_T}$ with $H_T = \sum_1^{n_j} p_T^j$. In signal events multiplicity of hard jets are expected to be higher than the SM processes, so $R_{\ell\ell}$ is likely to be distributed towards the lower values which is reflected in the suppression of $t\bar{t}$ background due to this $R_{\ell\ell}$ cut. An invariant mass($m_{\ell\ell}$) cut for OS lepton case is applied to suppress the background from Z decay. In table 3 we present the effects of each set of cuts described by eq.14 to the signal process for the parameter points A,B and C and as well as the backgrounds. The second and third columns present the production cross sections and number of events simulated in each case respectively and the subsequent rows show the suppression due to cuts. Clearly, the new cut $R_{\ell\ell}$ is killing backgrounds by a factor of two or more with a less effect on the signal events. We present the survived number of events with OS and SS sign leptons separately. Eventually, the last two columns display the predicted

number of signal and background events for luminosity $\mathcal{L} = 1fb^{-1}$ and $5fb^{-1}$ respectively. They are normalized to the cross-sections of second column. The last two columns show promising SS and OS di-lepton signals for point A, with a signal/background ratio >1 for the SS channel. They also show a moderate OS di-lepton signal for the point C at $3(5)\sigma$ level with $1(5)fb^{-1}$ luminosity data. There is no viable di-lepton signal for the point B.

Single lepton + jets + \cancel{E}_T : We simulate the signal events in the single lepton final states along with jets and \cancel{E}_T . In addition to the selection of single lepton with cuts of eq. 12, we apply the following cuts,

$$\begin{aligned} \text{Number of jets} &\geq 4 \text{ with } p_T^{j_1} \geq 100 \text{ GeV}, \\ m_T &> 70 \text{ GeV}, \cancel{E}_T > 150 \text{ GeV}, M_{eff} \geq 500 \text{ GeV}, \\ R_\ell &< 0.1 \text{ and } \geq 3 \text{ b-tagged jets}, \end{aligned} \quad (15)$$

where the transverse mass between lepton and \cancel{E}_T is defined as $m_T = \sqrt{2E_T^\ell \cancel{E}_T (1 - \cos \phi(\ell, \cancel{E}_T))}$ and $R_\ell = \frac{p_T^{\ell_1}}{\cancel{E}_T}$. In table 4 we show the event summary for this case like table 3. The last two columns show the number of events for the two values of luminosities and with ≥ 3 b-tagged jets in the final state. We have checked that without the ≥ 3 b-tags the signal and background sizes are very similar to the OS di-lepton case. The ≥ 3 b-tags effectively suppresses the background to $\leq 50\%$ of the signal, so that the viability of the signal is determined by the number of signal events. With $5fb^{-1}$ luminosity one expects ~ 10 signal events for the point A but only ~ 2 events for points B and C. With a luminosity of $15fb^{-1}$ expected in 2012 one would expect a viable signal of 5-6 events for the points B and C.

Jets + \cancel{E}_T : In the simulation for jets+ \cancel{E}_T channel, we select at least four jets where jets are selected applying cuts as described above. Moreover, we apply two new background rejection cuts following the paper of ref. [21]. One of them is the transverse thrust [22] as defined,

$$T = \max_{n_T} \frac{\sum_i |\vec{q}_{T,i} \cdot \vec{n}_T|}{\sum_i q_{T,i}}, \quad (16)$$

where the sum runs over all objects in the event, $\vec{q}_{T,i}$ is the transverse component of each objects and \vec{n}_T is the transverse vector which maximizes this ratio. Obviously, the events having larger multiplicities will predict smaller values of T than the values for the events with comparatively lower multiplicities [21]. The other variable is related with the ratio of scalar sum of transverse of momentum of jets i.e the ratio(R_T) between the scalar sum of p_T for required lowest number of jets (n_j^{min}) in the event and the scalar sum of p_T of all jets(n_j) present in the same event, i.e,

$$R_T = \frac{\sum_1^{n_j^{min}} p_T^{j_i}}{H_T} \quad (17)$$

Proc	C.S (pb)	N	Single lep.	n_j ≥ 4	m_T ≥ 70	\cancel{E}_T ≥ 150	M_{eff} ≥ 500	R_l ≤ 0.1	n_b ≥ 3	$1fb^{-1}$	$5fb^{-1}$
A: $\tilde{g}\tilde{g}$	5.84	10k	2270	570	308	143	98	42	7	1.25	6.25
A: $\tilde{q}\tilde{q}$	0.28	10k	1440	1222	684	523	519	387	56	0.6	3.0
A:Total										1.85	9.25
B: $\tilde{g}\tilde{g}$	0.06	10k	1987	1703	1208	865	789	440	136	0.4	2.0
B: $\tilde{q}\tilde{q}$	0.018	10k	2702	1867	1348	1153	1150	889	268	0.023	0.12
B:Total										0.42	2.12
C: $\tilde{g}\tilde{g}$	0.1	10k	1334	909	683	513	466	258	68	0.2	1.0
C: $\tilde{q}\tilde{q}$	0.57	10k	1057	957	459	330	301	214	12	0.2	1.0
C: $\tilde{q}\tilde{q}$	0.55	10k	882	266	198	139	135	59	2	< 1	< 1
C:Total										0.4	2.0
$t\bar{t}$											
5 – 200	143.52	100k	23255	1296	607	78	36	5	0	0	
200 – 500	16.32	50k	11196	2044	952	382	267	41	2	0.27	1.35
500 – inf	0.16	10k	2030	458	233	152	151	32	5	0.02	0.1
Total										0.29	1.45
QCD											
200-300	6986	1M	12413	0	0	0	0	0	0	0	
300-500	873	1M	1274	252	13	0	0	0	0	0	
500-800	43.1	100k	158	39	2	1	0	0	0	0	
QCD:Total											

Table 4: The signal and background events, same as table 3, but for single lepton final states. The last two columns show the number of events multiplied by proper b-tagging efficiency for two luminosity options.

with $H_T = \sum_1^{n_j} p_T^{j_i}$. Evidently, behavior of R_T distribution is very much dependent on the number of jets distributions and their respective hardness in the event. For instance, in the case of $n_j \sim n_j^{min}$ which is true for the SM backgrounds, $R_T \sim 1$ where as in the case of signal where $n_j \gg n_j^{min}$, R_T will be smaller than unity. Hence, T and R_T are very useful tool to suppress the SM backgrounds without affecting much the signals rates.

In our simulation for the jets+ \cancel{E}_T final states, we apply following set of event selection and background suppression cuts,

$$\begin{aligned} &\text{Number of jets} \geq 4; T \leq 0.95, R_T \leq 0.9 \\ &\cancel{E}_T \geq 200 \text{ GeV}; H_T \geq 500 \text{ GeV} \\ &\geq 3 \text{ b-tagged jets with } p_T \geq 30 \text{ GeV}, |\eta| \leq 2.5. \end{aligned} \tag{18}$$

In Table 5 we display event yield after each of the cuts for all the three parameter points A,B and C as described in table 1 and also for backgrounds. As before, the second and third column present the production cross sections and the number of events simulated for each processes respectively. Finally, the number of events normalized by luminosities are shown in the last two columns with ≥ 3 b-tagged jets in the final states. We see that the ≥ 3 b-tags effectively suppresses the background to $< 20\%$ of the signal, so that the viability of the signal is determined by its size. Moreover, with a luminosity of $5fb^{-1}$ we expect 50 signal events for point A and 15-16 events for points B and C. Therefore, one can probe the entire parameter space of this model up to a gluino mass of ~ 800 GeV.

4 Summary

We have analyzed the prospect of probing a non-universal gaugino mass model of mixed bino-higgsino DM at the current 7 TeV run of LHC. In contrast to the mSUGRA model this model can provide cosmologically compatible DM relic density over a large part of the parameter space. In particular it provides WMAP compatible DM relic density over two branches - (1) $m_{\tilde{g}} < m_{\tilde{q}}$ and (2) $m_{\tilde{g}} \sim m_{\tilde{q}}$ -where the DM annihilation occur via gauge boson and Higgs exchanges respectively. Moreover, the 1st branch offers promising signals for the forthcoming DM detection experiments due to nearly equal bino-higgsino components in the DM. On the other hand, the 2nd branch offers a larger signal at LHC due to the relatively light squarks. In contrast to the mSUGRA model, the SUSY mass spectrum of this model has two distinctive features -(1) an approximate degeneracy of the lighter chargino and neutralino masses and (2) an inverted hierarchy of the squarks masses. The 1st feature implies that the $\tilde{\chi}_1^0$ coming from the SUSY cascade decay carries a relatively large fraction of the energy-momentum, resulting in a hard missing transverse energy(\cancel{E}_T) distribution. The 2nd feature implies that the gluino decays preferentially to t and b quarks, leading to hard isolated leptons and multiple b-tags. In particular we have used the ≥ 3 b-tags requirement to effectively suppress the background, so that the viability of the signal is determined by the number of signal events. With a luminosity of $5fb^{-1}$, one expects a viable signal in the

Proc	C.S (pb)	N	T ≤ 0.95	R_T $\leq .9$	E_T ≥ 200	H_T ≥ 500	n_b ≥ 3	$1fb^{-1}$	$5fb^{-1}$
A: $\tilde{g}\tilde{g}$	5.84	10k	6900	3170	446	301	32	6.6	33.0
A: $\tilde{q}\tilde{q}$	0.28	10k	8332	4356	2042	2002	315	3.4	17.0
Total								10	50
B: $\tilde{g}\tilde{g}$	0.06	10k	8708	5901	2901	2584	779	2.07	10.35
B: $\tilde{q}\tilde{q}$	0.018	10k	9100	6263	4212	4177	1322	1.02	5.1
Total								3.09	15.45
C: $\tilde{g}\tilde{g}$	0.1	10k	7623	3700	2888	1761	404	1.13	5.65
C: $\tilde{q}\tilde{q}$	0.57	10k	5933	1984	1145	1030	121	1.82	9.1
C: $\tilde{q}\tilde{q}$	0.55	10k	3326	729	433	385	17	0.3	1.5
. Total								3.25	16.25
$t\bar{t}$									
5-200	143.5	100k	37162	14548	21	14	0	0	0
200-500	16.32	50k	27831	8559	109	54	3	0.48	2.4
500-inf	0.16	10k	1741	482	68	64	7	0.09	0.45
Total								0.57	2.85
QCD									
300-500	873	1M	194636	27532	7	5	4.3	0	0
500-800	43.1	100k	19100	2329	9	9	3.8	0	0
200-300	6983	1M	123	14	0	0	0	0	0

Table 5: The signal and background events after, same as table 3, but for jets+ E_T final states. The kinematic selection cuts are described in the text. The last two columns present the number of events with respective luminosities as shown.

inclusive jets+ \cancel{E}_T channel up to $m_{\tilde{g}} \sim 800$ GeV over both the branches. One can achieve this in the single lepton + jets+ \cancel{E}_T channel with a luminosity of $15 fb^{-1}$, which is expected at the end of the current run in late 2012. Without the ≥ 3 b-tags, one has to contend with a large background from $t\bar{t}$ production. In this case the single lepton and di-lepton channels offer viable signals up to $m_{\tilde{g}} \sim 800$ GeV over the 2nd branch ($m_{\tilde{g}} \sim m_{\tilde{q}}$) for a luminosity of $5 fb^{-1}$, while it goes only upto $m_{\tilde{g}} = 400\text{-}500$ GeV over the 1st branch ($m_{\tilde{g}} < m_{\tilde{q}}$).

5 Acknowledgment

The authors are thankful to Utpal Chattopadhyay for helping to compute the SUSY mass spectrum and Debottam Das for helping to make figure. DPR acknowledges partial support from the Indian National Science Academy through its senior scientist programme.

References

- [1] H. Baer, V. Barger, A Lessa and X. Tata, JHEP **1006**, 102(2010), arXiv:1004.3594[hep-ph].
- [2] For details, see ATLAS collaboration, <https://twiki.cern.ch/twiki/bin/view/AtlasPublic/SupersymmetryPublic>; CMS collaboration, <https://twiki.cern.ch/twiki/bin/view/CMSPublic/PhysicsResultsSUS>.
- [3] J. R. Ellis, K. Enqvist, D. V. Nanopoulos and K. Tamvakis, Phys. Lett. **B 155**, 381(1985); M. Drees, Phys.Lett **B 158**, 409 (1985).
- [4] G. Anderson, H. Baer, C.H.Chen and X. Tata, Phys. Rev.**D 61**, 095005(2000); K. Huitu, Y. Kawamura, T. Kobayashi, and K. Puolamaki, Phys. Rev. D61,035001 (2000).
- [5] U. Chattopadhyay and D. P. Roy, Phys. Rev. **D 68**, 033010 (2003).
- [6] S. F. King, J. P. Roberts and D. P. Roy, JHEP **0710**, 106 (2007).
- [7] U. Chattopadhyay, D. Das and D. P. Roy, Phys. Rev. **D 79**, 095013(2009).
- [8] D. P. Roy, Phys Rev. **D 81**, 057701(2010).
- [9] M. Carena, M. Olechowski, S. Pokorski, and C.E. Wagner, Nucl. Phys. **B426**, 269 (1994); S. Komine and M. Yamaguchi, Phys. Rev. **D63**, 035005 (2001).
- [10] C. Amsler et. al. [Particle data Group], Phys. Lett. **B 667** 1(2008).
- [11] E. Komatsu et. al. [WMAP collaboration], Astrophys.J.Suppl.Ser. **180**, 330(2009).
- [12] N. Arkani-Hamed, A. Delgada and G.F.Giudice, Nucl. Phys. **B 741**, 108(2006).

- [13] Z. Ahmed et al. [CDMS Collaboration], Science **327**, 1619(2010).
- [14] E. Aprile et. al. [XENON 100 Collaboration], arXiv:1104.2549[astro-ph].
- [15] A. Djouadi, J.L.Kneur and G. Moultaka, Compt Phys. Comm, **176**,426(2007); A. Djouadi, M.M.Muhlleitner and M. Spira, ACTA Phys, Polon, **B38**,635(2007).
- [16] W. Beenaker, R. Hopker, M. Spira and P. Zerwas, Nucl Phys. **B 492**,51(1997).
- [17] T. Sjostrand, S. Mrenna and P.Z. Skands, JHEP, **05**, 026(2006), arXiv:hep-ph/0603175.
- [18] PGS4, J. Conway et. al. For details, see, <http://physics.ucdavis.edu/conway/research/software/pgs/pgs4-general.htm>
- [19] CMS Collaboration, CMS PAS BTV-11-001.
- [20] N. Kidonakis, arXiv:1109.3231[hep-ph].
- [21] M. Guchait and D. Sengupta, Phys, Rev **D84**, 055010(2011), arXiv:1102.4785[hep-ph].
- [22] A. Banfi, G. P. Salam and G. Zanderighi, JHEP **1006**, 038(2010), arXiv:1001.4082[hep-ph].